

This is the accepted manuscript of the contribution published as:

Krueger, J., Heitkötter, J., Leue, M., **Schlüter, S., Vogel, H.-J.**, Marschner, B., Bachmann, J. (2018):

Coupling of interfacial soil properties and bio-hydrological processes: The flow cell concept
Ecohydrology **11** (6), art. e2024

The publisher's version is available at:

<http://dx.doi.org/10.1002/eco.2024>



Coupling of interfacial soil properties and bio-hydrological processes:

The Flow Cell Concept

Jiem Krueger^{1*}, Julian Heitkötter², Martin Leue³, Steffen Schlüter⁴, Hans-Jörg Vogel⁴, Bernd Marschner², Jörg Bachmann¹

Special issue Biohydrology

* corresponding author: Jiem Krueger, krueger@ifbk.uni-hannover.de

Phone: +49 (0)511 762 19250

Fax: +49 (0)511 762 5559

¹Leibniz Universität Hannover, Institute of Soil Science, Herrenhäuser Straße 2, 30419 Hannover, Germany

²Ruhr-Universität Bochum, Institute of Geography, Soil Science/Soil Ecology, Universitätsstraße 150, 44801 Bochum, Germany

³Leibniz Centre for Agricultural Landscape Research, Eberswalder Straße 84, 15374 Müncheberg, Germany

⁴Department of Soil System Sciences, Helmholtz Centre for Environmental Research - UFZ, Theodor-Lieser Straße 4, 06120 Halle (Saale), Germany

This article has been accepted for publication and undergone full peer review but has not been through the copyediting, typesetting, pagination and proofreading process which may lead to differences between this version and the Version of Record. Please cite this article as doi: 10.1002/eco.2024

Abstract

By applying the newly developed flow cell (FC) concept, this study investigated the impact of small scale spatial variations (mm to cm) in organic matter (OM) composition (diffusive reflectance infrared Fourier transform (DRIFT) spectroscopy), biological activity (zymography), and wettability (contact angle, CA) on transport processes (tracer experiments, radiography). Experiments were conducted in 5 undisturbed soil slices (mm apart), consisting of a sandy matrix with an embedded loamy band.

In the loamy band increased enzyme activities and OM (10 mm apart) were found compared to the sand matrix, with no interrelations although spatial autocorrelation ranges were up to 7 cm. CAs were increased (0-110°) above the loamy band and were negatively correlated with acid phosphatase. Missing correlations were probably attributed to texture variations between soil slices. A general correlation between CA and C content (bulk) were confirmed. Variability in texture and hydraulic properties led to the formation of heterogeneous flow patterns and probably to heterogeneously distributed interfacial properties.

The new FC concept allows process evaluation on the mm scale to analyze spatial relations, i.e. between small scale textural changes on transport processes and biological responses. The concept has been proved as a versatile tool to analyze spatial distribution of biological and interfacial soil properties in conjunction with the analysis of complex micro-hydraulic processes for undisturbed soil samples. The concept may be improved by additional non-destructive imaging methods which is especially challenging for the detection of small scale textural changes.

Keywords: undisturbed soil, Flow Cell, transport processes, DRIFT spectroscopy, extracellular enzyme activity, soil water repellency, X-ray radiography

Introduction

Water and nutrient availability in soils is strongly affected by physical and physico-chemical characteristics of pore surface properties such as surface charge, surface free energy, and pore space attributes (pore size, tortuosity, and connectivity). Water flow governs the convective nutrient and enzyme transport and microbial mobility within the soil profile. The heterogeneous nature of the soil pore network plays a fundamental role in determining microbial abundance, activity, and community composition by affecting the relative proportion of air- and water-filled pores and their dynamics with changing soil water content. These biogeochemical processes, in turn, regulate water and nutrient availability, gas diffusion, and biotic interactions (e.g. Thecon & Or, 2017). Microbial activity is maximized (respiratory output) when about 60 % of the total pore space is water filled (Or et al., 2007; Frey, 2007).

Below this level, water-filled pores become poorly interconnected, water circulation becomes restricted, and dissolved nutrients become less available for microbial utilization (Frey, 2007). Dynamic variations in water availability in soil, in time and space, affect the diffusion processes that determine the spatial and temporal distribution of microbial communities and activities (Koch, 1990). Decoupling of biological and physical processes, i.e. physical separation of biological activity and organic matter (OM), is apparently one of the most important factors leading to the protection and stabilization of soil organic matter (SOM) in subsoils (Or et al., 2007). The microbial release of enzymes plays an important role for the decomposition of OM in soils. The presence of specific enzymes from different nutrient cycles provide general information about microbial activity and further reflect the needs and the decomposition potential of the microorganisms in soil (Burns et al., 2013; Caldwell, 2005).

Due to the formation of organic coatings, the functional groups of soil organic matter (SOM) adsorbed on particle surfaces are most likely responsible for chemical reactivity and sorptiv-

ity and determine basic physico-chemical properties of particle surfaces such as wettability (Capriel et al., 1995; Chenu et al., 2000; Woche et al., 2017). Soil water repellency (SWR) may lead to inhomogeneous distribution of water and promote preferential flow pathways due to enlarged spatial variability (Bauters et al., 2000; Dekker et al., 2001; Dekker & Ritsema, 1994) which exclude large areas from water and nutrient flow (Doerr et al., 2000; Goebel et al., 2007, 2011) and therefore can cause reduced microbial activity in soils (e.g. Goebel et al., 2007). Preferential flow pathways can persist for decades and along these pathways, soil organic carbon (SOC) and nitrogen concentrations and microbial activity were found to be higher than in the surrounding soil matrix due to a better nutrient supply as observed for a spruce-beech forest (Bundt et al., 2001a, b). Seasonal drying of forest soils enhances SWR (Buczko et al., 2005; Krammes & DeBano, 1965) which directly affects temporarily local soil hydraulic processes like surface runoff, infiltration behavior, and sorptivity (Clothier et al., 2000). These processes might further significantly affect water dynamics from the local to the catchment scale (Doerr et al., 2003). SWR is not only restricted to topsoil and was also reported for subsoil (Woche et al., 2005; Bachmann et al., 2016). Spatial variable SWR does not only exist at the profile (i.e. m-to-cm) scale, but also on the mm-scale (Lamparter et al., 2010; Bachmann et al., 2013).

Particle coatings of SOM compounds containing significant amounts of nonpolar functional groups (Bisdorf et al., 1993; Capriel et al., 1995; Ellerbrock et al., 2005), originating from plants and roots (e.g. Mao et al., 2014), fungi (McGhie & Posner, 1980; Ma'shum & Farmer, 1985) or microbial residues are known to generate SWR. The strength of SWR is frequently associated with the quantity of bulk SOC (Täumer et al., 2005; Mao et al., 2014), while other studies found no significant correlation of SOC to SWR (e.g. Doerr et al., 2000; Woche et al., 2005; Bachmann et al., 2016), only in some specific cases SWR could be explained by SOC content alone (e.g. Horne & McIntosh, 2000). This suggests that the type and orientation of

SOM functional groups rather than bulk SOC content determines SWR (e.g. Ellerbrock et al., 2005; Woche et al., 2017). However, these studies used a one-grain-layer of soil transferred to double sided adhesive tape, which had caused disturbances of the original spatial arrangement of the soil particles due to sample preparation. Recently, Krueger and Bachmann (2017) developed a new sampling technique that allows determination of SWR on the original undisturbed soil surface in mm steps. Such small-scale heterogeneity cannot be considered when analyzing disturbed soil samples.

Many of the effects described here cannot be detected on the basis of conventional soil column flow experiments, usually conducted in order to study soil hydraulic or soil-solution exchange processes (e.g. Carstens et al., 2017). The sampling technique developed by Krueger and Bachmann (2017) allows the analysis of undisturbed rectangular parallel samples (5 mm distance). The samples are certainly physically more similar, regarding spatial heterogeneity than cylindrical soil cores taken conventionally at dm distances. In their work, spatial dependencies (autocorrelation ranges, calculated by geostatistical tools) up to 7.2 cm were found for loamy topsoil sample. Compared to conventional column systems, only small amounts of material are needed while still maintaining a large observation area and maintaining a quasi 2D flow field during percolation.

The objective of the flow cell (FC) concept is to combine the new sampling method introduced by Krueger and Bachmann (2017) as a tool to characterize transport processes and surface properties on the mm-to-cm scale in undisturbed soil under controlled (temperature, capillary pressure, ambient gas composition) laboratory conditions. The specific objective of this study is to investigate on one hand the impact of texture heterogeneities on the spatial distribution of physico-chemical and chemical particle surface properties. On the other hand we focused on corresponding spatial pattern of biological activity. The analyzed soil slices had the advantage of a maximum distance of 10 mm from slice center to slice center of the

adjacent sample. Due to the small distances between the measured parameters, observable relationships and spatial dependencies were expected between physico-chemical, chemical and biological properties. Based on these interrelations links can be drawn and would improve our understanding of bio-hydrological processes in soil.

In our study we used this technique for the analysis of: i) tracer and water flux experiments, ii) small-scale mapping of wetting properties in terms of contact angle (CA), iii) mapping of extracellular enzyme activities by zymography and iv) analysis of the distribution of SOM functional groups via diffuse reflectance infrared Fourier transform (DRIFT) spectroscopy at undisturbed soil samples from a beech forest subsoil. In this way, the physico-chemical heterogeneity of (close to) undisturbed soil could be linked to transport properties and biological activity.

Material and Methods

Study site and soil sampling

Soil samples were taken at the beech forest stand 'Grinderwald' (*Fagussylvatica* L.) near Hanover, Germany (52° 34'22,115 North, 9° 18' 49,762 East). The Dystric Cambisol (IUSS Working group, WRB 2014) is characterized by a homogeneous sandy substrate in the top meter with some loamy-silty lenses and locally some gravel and stone layers in the more heterogeneous subsoil. Basic soil properties are given in Table 1. The FC sampling site of the present study is closely located to the three subsoil sampling locations used for larger scale (m) analysis of soil wettability described by Bachmann et al. (2016).

Undisturbed rectangular soil samples had been taken from the subsoil (68-79 cm depth) with the new field sampling method introduced by Krueger and Bachmann (2017) (Fig. 1).

The thin parallel soil slices obtained with this technique allow the analysis of undisturbed surfaces that are apparently more similar (5 or 10 mm distance, Krueger and Bachmann, 2017). With one sampling frame 5 subsamples (termed as “A” to “E”) of 5 and 10 mm thickness were obtained (Fig. 1). All subsamples had a brownish structure more or less in the center of the sample with an area of approximately 39 cm² embedded in a less brownish (yellow) sandy matrix. Photographs of subsample surfaces (opposite surfaces) and the measurement scheme are shown in Figure 2.

Spatial distribution of enzyme activity (slice B)

Soil zymography was performed according to Spohn and Kuzyakov (2014) in order to identify local hotspots with enhanced extracellular enzyme activities within the undisturbed soil surface in situ (field moist) of soil slice B. For our study the method was appropriate with some modifications concerning incubation time and drying time of soaked filters. The activity of β -glucosidase (β -Glu), N-acetylglucosaminidase (N-Acet) and acid phosphatase (Phos), involved in C-, N-, and P-cycle was analyzed separately (in this order).

Enzyme activity was determined by using fluorescent methylumbelliferyl(MUF)-substrates for each enzyme to visualize the enzymatical hydrolyzation during incubation. The substrates 4-MUF phosphate disodium salt (Phos), 4-MUF- β -D-Glucoside (β -Glu), and 4-MUF-N-Acetyl- β -D-Glucosaminide (N-Acet) were dissolved in millipore water containing 5 % (v/v) methanol to the desired concentration of 12 mM. Cut polyamide filters (Sartorius Ag, Göttingen, Germany), soaked in substrate solution were dried on aluminum foil for 1 minute. First a 1-mm-thick-layer of agarose gel (1 % agarose), was transferred to the soil slice surface (slice B, 75 x 100 x 10 mm, Fig. 2) and subsequently covered with substrate-soaked polyamide filter which had covered an area of 56.9 x 80.5 mm (x = 4.5-61.4 mm, y = 23-113.5 mm from slice B bottom left). The prepared soil slice was incubated for 1 h at 25 °C in the dark. Fur-

ther, a control was set for each substrate by placing a substrate-soaked membrane on an agarose plate which was then incubated under the same conditions as described above to determine the autofluorescence. After incubation, the polyamide filter was photographed (pixel resolution: $\sim 85 \mu\text{m}$) in a gel-documentation system (Biostep GmbH, Burkhardtsdorf, Germany) with epi-UV illumination at 365 nm and with a Canon camera EOS-700D equipped with a fixed focal length lens (F/1.8) and 420 nm filter. This determination was repeated separately for each enzyme activity. Image processing was performed with the Fiji-bundle for the open source software ImageJ (Schindelin et al., 2012). Gray values were multiplied by a factor of 6 to get higher contrast and the autofluorescence of the respective substrate was subtracted and were converted with a calibrated color scale in picomoles (μM) substrate hydrolyzed per mm^2 and hour.

Spatial distribution of SOM functional groups with DRIFT mapping (slice C)

The spatial distribution of SOM composition in terms of the specific infrared (IR) absorbance of functional groups was analyzed via DRIFT spectroscopy by 2D-mapping of the intact surface of slice C (Fig. 2). Measurements were carried out with a FTIR spectrometer (BioRad FTS 135, Digilab, Randolph, MA, USA) coupled with a xy-positioning table (Leue et al., 2010b). The soil slice was cut to a reduced size of 120 by 75 mm, suitable for the xy-positioning table. Prior to analysis, the soil slice was desiccated (at relative humidity 30 %, 20°C) to mass constancy in order to minimize moisture content effects on the DRIFT spectra.

The focus of the IR device was adjusted to the surface elevation of the soil slice; the diameter of the IR beam was 1.5 mm. Each spectrum was recorded by 16 co-added scans between wave numbers (WN) 4000 and 400 cm^{-1} at a resolution of 4 cm^{-1} and related to a background spectrum measured on a gold-target (99 % Infragold, Labsphere, North Sutton, NH, USA).

The grid was measured in steps of 5 mm along 13 parallel transects of 90 mm length with

5 mm distance resulting in a 90 x 60 mm grid size ($n = 920$, $x = 3-63$ mm, $y = 25-113$ mm from slice C bottom left). Spectra were converted to Kubelka–Munk (KM) units, smoothed by a boxcar moving average algorithm of factor 7, and corrected for baseline shifts using the software WIN-IR Pro 3.4 (Digilab, Massachusetts, USA) and were normalized to maximum intensity ($WN\ 1351\ cm^{-1}$). DRIFT signal intensities of summed bands of $WN\ 1983\ cm^{-1}$ and $WN\ 1873\ cm^{-1}$ (Sum Si-O) were evaluated as parameter for Si-O overtones and combination bands indicative for the particle size: higher values, i.e. higher reflectance, were indicative for relative smaller particles (Leue et. al, 2010a).

The potential wettability index (PWI; Leue et al., 2013) as the ratio between DRIFT signal intensities of summed C-H (Sum C-H) stretching vibrations of alkyl groups (hydrophobic), and the signals of summed C=O (Sum C=O) groups of carbonylic (hydrophilic) OM groups was determined (Ellerbrock et al., 2005). Higher PWI values indicate lower wettability. For each spectrum the signal intensities of C-H groups between $WN\ 2948-2920\ cm^{-1}$ and $2864-2849\ cm^{-1}$ were analyzed as vertical distance from a local baseline. The signal intensities of C=O and C=C groups, between $WN\ 1720-1700\ cm^{-1}$ and $1625-1600\ cm^{-1}$, as well as the Si-O groups, were measured as height from the total baseline of the spectra (Ellerbrock et al., 2005). Spatial differences between Sum Si-O, Sum C=O and Sum C-H were verified by the one-sample t-Test. For non-normally distributed data or unequal variances Mann-Whitney Rank Sum Test instead, were performed (Tab. 3) for values of 13 spectra of 3 horizontal lines (marked in Fig. 5) of 10, 45 and 85 mm (MI, Band, MII, Fig. 5).

Bulk soil measurement (subsamples of slice C)

Subsamples were excavated after DRIFT measurements from slice C in form of cylindrical cores with 20 mm diameter (volume of $1.57\ cm^3$, Fig. 5). This resulted in 12 subsamples, each homogenized separately for the following bulk soil analyses.

C and N analyses were performed by dry combustion with a CNS-Elemental Analyzer (Vario EL III, Elementar Analysensysteme GmbH, Hanau, Germany) for all homogenized subsamples of slice C.

Soil wettability was determined in terms of contact angle (CA) measurements. Homogenized subsample material of slice C was fixed as an ideally one-grain layer on a glass slide with double-sided adhesive tape with the sessile drop method (SDM) as described in Bachmann et al. (2000). The initial CA were analyzed after placement of the water drop and ending of mechanical disturbances by drop shape analysis (ellipsoidal fit) and fitting of tangents on the left and right side of the drop with the software SCA 20 (DataPhysics, Filderstadt, Germany). The arithmetic mean value of 6 analyzed drops (12) was used for further evaluation.

The chemical compositions of particle surfaces were analyzed by X-ray photoelectron spectroscopy (XPS) with a maximum analysis depth of 10 nm. Five subsamples of soil slice C (1, 3, 4, 8 and 12, see Fig. 5) were chosen exemplary. Spectra were recorded with an Axis Ultra DLD instrument (Kratos Analytical, Manchester, UK) using monochromated Al-K α radiation (1486.6 eV). The samples were fixed with ultrahigh vacuum-stable carbon conductive tape (Agar Scientific Elektron Technology UK Ltd., Stansted, UK) on a sample bar with a sample area of about 50 mm². Three survey spectra, in the binding energy (BE) range of 1200-0 eV were recorded at three different measurement positions per sample (n = 3) with a resolution of 1 eV. The pass energy was 160 eV, the high voltage 12 kV, and the emission current 20 mA. The takeoff angle of the emitted photoelectrons was 0° and the measured area in the slot modus 0.21 mm² (300 × 700 μm). Three sweeps with a dwell time of 500 ms were performed for each measurement. The neutralizer was active during the measurements to compensate for sample charging, resulting from emission of photoelectrons from non-conductive material like soil by flooding the surface with low energy electrons. Nevertheless, charging could not be prevented completely and all spectra were corrected to Si 2p BE (103 eV, Si in

quartz; e.g., Okada et al., 1998). The spectra were analyzed with the software Vision 2 (Kratos Analytical, Manchester, UK) and the mean surface elemental composition was given in atomic concentration (at.-%).

Estimations of polar and nonpolar C species amounts were conducted with two subpeaks defined to the C 1s peak of the survey spectra, one with a BE around 285 eV representing polar C species (C_p) and the other with a BE around 284 eV representing nonpolar C species (C_{np} , Krueger et al., 2016; Woche et al., 2017). The BE difference was fixed to 1 eV. For both peaks Gaussian distributions were assumed and peak asymmetry was allowed due to several C species contributing to the respective peak while the full-width-at-halfmaximum values were kept similar for both peaks. For peak fitting the software eXPFit (Version 1.5 for Excel 2007) were used.

Spatial distribution of wettability (slice D)

The small scale spatial variability of soil wetting properties was assessed by CA mapping on the undisturbed soil surface of slice D. Data were taken from Krueger and Bachmann (2017). Droplets of 1 μ L were found to be appropriate for regular CA mapping of a 3 x 3 mm grid. The intact surface of slice D was mapped along horizontal lines in 3 mm and parallel spacing of 3 mm between the transects (grid size 56 x 90 mm, x = 5-61 mm, y = 25-115 mm from slice D bottom left, Fig. 2).

Statistical data evaluation

Descriptive statistics and linear correlations of data were calculated according to standard methods performed with SigmaPlot (Systat Software GmbH, Erkrath, Germany). The spatial variability of data was evaluated by geostatistics as follows: contour plots were predicted by

point kriging interpolation based on calculated semivariances with no directional differences (isotropic) with the software GS+ (Version 9.0, Gamma Design Software, Plainwell, Michigan, USA) which resulted in kriged contour plots with a data resolution of 0.8 x 0.8 mm. In semivariogram analysis, the sill represents the maximum (total) variation (model asymptote), and nugget variance, the y-intercept of the model represents the random variation for samples approaching zero distance (nugget effect). Subtraction of nugget from sill results in the auto-correlated variation. The separation distance over which spatial dependence is apparent is the range of autocorrelation where the model reaches the sill (Webster and Oliver, 2001; Nielsen and Wendroth, 2003). Semivariances ($\gamma(h)$) were calculated for a distance (lag, h) depending on minimum distance to measurement points, with a maximum separation distance of 80 mm and a separation angle tolerance of 22.5°. Semivariogram models (exponential, spherical and pure nugget) were fitted to a maximum correlated separation distance to each data individually to the sample semivariograms. The quality of the model fit was characterized by comparing correlation coefficients (r^2).

As a basic principle we used the results of geostatistical interpolation for the calculation of interrelationships (Pearson, correlation coefficient, R^2) of the mapped data. Due to the differences in the measurement grid sizes, it was necessary before the analysis to calculate spatial correlation ranges to overcome the problem of missing data between measurement points. In this way, different properties measured at different resolution could be related.

Transport experiments (slice E)

Flow Cell Preparation

Repeated infiltration experiments were performed in unsaturated intact soil samples to visualize and to detect preferential flow path ways and their stability. Experiments of this study were conducted with slice E (75 x 103 x 10 mm).

A layer of HCl-washed, high purity quartz sand (grain size: 45 % 0.1-0.2 mm, 53 % 0.2-0.315 mm, and 1 % for < 0.1 mm and > 0.315 mm; Carlo Bernasconi AG, Bern, Switzerland) was prepared at the top (height 25 mm) and bottom (height 10 mm) of the soil slice to ensure hydraulic contact between membrane box and soil. The prepared flow cell (FC) had a total height of 138 mm and a volume of 103.5 cm³. Then membrane boxes, composed of transparent acrylic glass with an external size of 20 or 50 mm height, 75 mm length, and 10 mm width (Fig. 3, left), were inserted at the top and bottom of the FC. The in/outlet of the membrane box had a diameter of 5 mm and was connected to a tube (inner diameter 1.1 mm). The equally distributed 13 out/inlets at the bottom had a diameter of 2 mm with a total area of 40.84 mm² and were connected with a membrane of 5 µm mesh size. A maximum flow rate of about 5 ml min⁻¹ and an air entry pressures from zero down to -100 hPa could be adjusted with the membrane boxes.

Experimental set up

Infiltration experiments into unsaturated soil were conducted with a hanging water column adjusted via the membrane boxes with boundary conditions (BC) of +1 hPa at the top and -40 hPa at the bottom of the FC for all infiltration experiments. To prepare the initial moisture content, a defined initial moisture profile was achieved by infiltration in horizontally lying FCs with 0.01 M CaCl₂ solution, with upper BC of -1 hPa and lower BC of -10 hPa until

steady-state flux occurred. After steady-state flux was reached (assumed constant moisture profile) the infiltration was stopped and the FC was positioned vertically and was drained (24 hours) supported by a hanging water column adjusted at the bottom of the FC of -40 hPa while a no-flux boundary condition controlled the top. After the adjustment of initial water content 3 infiltration experiments were conducted as follows:

- i) After percolation with background solution (0.01 M CaCl₂) until steady-state, Brilliant Blue FCF (negatively charged organic molecule) solution (0.5 g l⁻¹, BB; C₀) of 1 pore volume (PV, 43 cm³) was applied. Subsequently the sample was rinsed with 0.01 M CaCl₂ solution (14 PV). Effluent volumes of approx. 4 ml were collected with an automated fractionation collector (Fig. 3, Bromma 2070 Ultra Rac II, LKB Instruments Inc., Rockville, USA). The experimental set up is shown in Figure 3. BB concentration was determined via UV/Vis spectroscopy (Cary 50 Scan, Varian Inc., USA) at 630 nm, using a regression equation derived from a BB calibration. The breakthrough curve (BTC) was determined using the tracer concentration C measured in the leachate in relation to C₀ (C/C₀) versus the number of eluted PVs. The soil hydraulic transport parameters were estimated with STANMOD (Šimůnek et al., 1999). Nonpolar sites of the molecule would preferentially be adsorbed to organic matter (Germán & Flühler, 2000).
- ii) Prior to infiltration of 1 PV of 0.01 M CaCl₂ solution the sample was oven-dried (30°C, 24 h). The percolation was running until the effluent reached constant flux. Afterwards the FC was oven-dried again (30°C, 24 h).
- iii) For radiography, a tracer solution of 20 g l⁻¹ KI and 0.5 g l⁻¹ BB was applied as pulse infiltration of 1 PV to achieve detectable density changes in the FC. Subsequently the

sample was rinsed with 2 PV 0.01 M CaCl₂ solution until the effluent reached constant flux.

Afterwards the FC was oven dried at 105° C for 24 h to measure bulk density and to calculate total porosity.

Immediately after application of the solution for infiltration ii) and iii), 8 radiographical images were taken with an exposure time of 708 ms in 60 s time steps. Absorption measurements were conducted by a polychromatic X-ray microtomograph (Nikon, Metrology X-Tek XCT 225) with a 12-bit CCD panel detector. Images were acquired at an energy level of 90 kV and 600 μA and 0.2 mm copper filter. The FC was placed between X-ray source and detector with a resultant effective pixel size of about 64 μm. The gray values in the radiographs were normalized with a two-point calibration using the average gray value within a test area along the acrylic wall and another test area within the empty exterior. The radiographs of each time were registered to the radiograph of the initial state prior to infiltration with the TurboReg Registration Tool (Thevenaz et al., 1998) to correct for small spatial drifts over time. Finally the initial image was subtracted from each radiograph. The difference images display the added X-ray attenuation caused by the infiltrating solution in arbitrary units. Image processing was performed with the Fiji-bundle for the open source software ImageJ (Schindelin et al., 2012).

Results

Spatial distribution of enzyme activity (slice B)

Figure 4 shows a photograph of soil surface and the results of measured enzyme activities.

The sample surface had some heterogeneity in color (by visible inspection), i.e. a brownish colored region in the middle of the sample was somehow embedded in a less colored matrix.

Regarding spatial analysis of the exo-enzymes, spherical models were fitted to all semivariograms with r^2 of about 0.99. For spatial analysis geostatistical evaluation revealed calculated autocorrelation ranges of 37 mm for N-Acet, 40 mm for Phos and largest ranges of 42 mm for β -Glu (Tab. 2).

The measured extracellular enzyme activities showed a heterogeneous spatial distribution within the surface of slice B (Fig. 4). Generally higher enzyme activities were found mainly in the region and immediate vicinity of the brownish colored region (Fig. 4), with N-Acet having the lowest enzyme activities in the range of 0-10 $\mu\text{M mm}^{-2} \text{h}^{-1}$ and Phos the highest enzyme activities with ranges mainly between 10 and 25 $\mu\text{M mm}^{-2} \text{h}^{-1}$. Areas with increased enzyme activities (> 12 -25 $\mu\text{M mm}^{-2} \text{h}^{-1}$) were found at two locations for all three analyzed enzymes (Fig. 4, marked in black). These 'hotspots' of apparently higher C, N, and P turnover were located directly above the brownish colored region. Also, 2 regions with reduced enzyme activities around 0-5 $\mu\text{M mm}^{-2} \text{h}^{-1}$ were found for all measured enzymes at the top and bottom of the soil slice.

Generally, soil zymography clearly visualized hotspots of enzyme activities within the undisturbed soil slice surface.

Spatial distribution of SOM functional groups with DRIFT mapping (slice C)

DRIFT results are presented as kriged contour plots in Figure 5. The photograph includes the coordinates of the measured grid as black points. By visible inspection, the sample had a brownish colored region; the color embedded in a less colored matrix as the soil slice B.

The calculated semivariograms used to compute the kriged contour plot, revealed no spatial dependency on the measured scale (pure nugget model, Tab. 3) neither for Sum C-H nor for the PWI values. Spherical models were fitted for semivariograms of Sum Si-O and Sum C=O with r^2 of 0.997 and 0.995, whereby calculated autocorrelation ranges were larger for Sum Si-O with 78 mm than for Sum C=O with 51 mm.

The results of DRIFT measurements generally showed higher signal intensities of OM groups (alkyl groups; Sum C-H, carboxylic and carbonylic groups; Sum C=O) as well a slightly higher PWI values in the brownish colored region (Fig. 4, photo) compared to the rest of the sample with values of Sum Si-O between 0.85 and 1. On the contrary, values of Sum Si-O and C=O were relatively lower in regions above and below the brownish colored region with values < 0.85 for Sum Si-O and < 1.1 for Sum C=O. PWI was mostly below 0.0025, only a few local PWI values were higher, corresponding to regions with higher Sum C-H values (Fig. 5).

The heterogeneously distributed DRIFT signal intensities of Sum Si-O were indicative for spatial variations in particle size; relatively higher values (higher reflectance) corresponded to smaller particle sizes. Mean values and standard deviations (SD) were given in Table 2. Means of Sum Si-O and Sum C=O were slightly higher for Band compared to MI and MII. No differences were found for small mean values of approx. 0.002 for Sum C-H for the three horizontal lines. PWI values were slightly increased from MI to MII with 0.0012 ± 0.0004 to 0.0018 ± 0.0008 . The mean values of Sum Si-O ($p = 0.007$) of MI/MII and Sum C=O ($p = 0.001$) of MI/Band and Sum C-H ($p = 0.024$) of MII/Band were significant different.

Highly significant differences were revealed for MI/Band and MII/Band for mean values of Sum Si-O and Sum C=O for MII/Band ($p < 0.001$). PWI values showed no differences for the three horizontal lines.

Bulk soil measurement (subsamples of slice C)

Surface particle coatings which are able to reduce wettability were analyzed by XPS on five bulk soil samples (Fig. 6). Quantification revealed a surface C content between 14.7 and 20.9 at.-% with highest contents in the sand matrix above the brownish structure between 15.5 and 20.9 at.-% (subsamples 4, 8, and 12, Fig. 6, Tab. 4). Lowest value with 14.7 at.-% was analyzed for subsample 3 in the brownish region. The proportion of C_{np} as related to C content was lowest for subsample 8 with 11.3 % and highest for subsample 1 with 41.4 %.

Subsamples 3, 4, and 12 varied around 34 %, thus indicating no relation between the amount of C_{np} and subsample origin, i.e. sand matrix or brownish structure. Furthermore, surface O/C ratios between 2.69 and 4.13 showed no distinct relation to the origin of the subsample (i.e., sand matrix, brownish structure).

Conventional C_{bulk} contents for 12 subsamples of soil slice C were low and ranged between 0.068 and 0.129 % and were spatial irregularly distributed. Slightly higher values were found above and in the brownish region with mean values around 0.1 %.

The determination of bulk CAs for 12 subsamples of soil slice C revealed wettable surfaces ($< 90^\circ$) with CA between 33° and 65° with relatively smaller CAs in the region of the brownish structure (i.e. 32° - 36° ; Fig. 6). No substantial correlations for surface C, C_{np} , C_p or O/C ratio with CA_{bulk} measured on disturbed soil particles were found. The variation of CA_{bulk} in this study was too small for any interrelations, i.e. for relations between wettability and sur-

face C content. We found a positive correlation between bulk CAs and C_{bulk} . ($r^2 = 0.766$) for subsamples of soil slice C.

Spatial distribution of wettability (slice D)

Similar to the slice C, the sample surface of slice D had a brownish colored region in the middle of the sample which was somehow embedded in a less colored matrix (by visible inspection, photograph Fig. 7).

The determined CAs on intact surface of slice D were heterogeneously distributed (Fig. 7).

The results revealed a differentiation into two regions with different wettability. The main part of the sample on the intact surface of slice D was wettable with CAs between 0° and 40° .

The upper part of the sample surface, slightly above the brownish structure, showed CAs in a wide range between 0° and 110° . These results had been already presented in Krueger and Bachmann (2017). The calculated semivariogram of Krueger and Bachmann (2017), predicted for the kriged contour plots, revealed a spatial correlation range of 4.5 cm on the measured scale (Tab. 3).

Transport experiments (slice E)

Soil slice E showed similar to the other slices differently colored regions by visible inspection, i.e. the brownish structure was again embedded in less-colored matrix.

To detect the general transport behavior of solutes and dissolved organic matter (DOM), break-through curves (BTC) were conducted with BB for infiltration i). The experiment was conducted with an initial average volumetric water content θ (-) of 0.34 and with a mean Darcy flow velocity of $0.8 \pm 0.001 \text{ ml min}^{-1}$. After infiltration, θ raised slightly to 0.36. The photographs in Figure 8 show the tracer pattern of BB after 1, 30, 60, 80, 200 and 300 min.

The moderate reactive tracer BB (anionic molecular structure) was distributed around the brownish structure (tracer exclusion), resulting in an unstable wetting front and a somehow fingering flow in the sand matrix (Fig. 8). At the end of the breakthrough experiment the tracer surrounded the brownish structure probably due to mobile/immobile transport domains indicating preferential flow leading to extended hydrodynamic dispersion. The photographs show also that non-affected areas are getting smaller with time by lateral transport from the entire interface to the sandy matrix.

After the tracer pulse, rinsing with CaCl_2 -solution led to decrease of dye intensity, i.e. a visual loss of color density in the BB flow pathways, while a colored fringe remained in the transition zone to the brownish structure (see photograph 200 and 300 min, Fig. 8).

Relative concentrations (C/C_0) were plotted against eluted PVs (Fig. 9). Highest relative BB concentrations were reached at 3.6 PV with $C/C_0 = 0.71$, then C/C_0 decreased relatively steep and reached a minimum of 0.16 after 4 PVs. This value was stable after overall 14 eluted PVs (not shown).

A slightly asymmetrical breakthrough curve with short tailing was derived for BB infiltration. The breakthrough characteristic was not strongly indicative for the presence of preferential flow, i.e. some areas were excluded from liquid transport (Fig. 8) leading to early breakthrough (< 1 PV) of the BB. Total breakthrough of 74.9 % of BB was determined, thus 25.1 % of BB remained in the soil slice. Model parameters for the BTC resulted in a low retardation coefficient for BB of 3.75 ± 0.065 and a Péclet number of 23.58 ± 4.084 . The Péclet number and the mean pore-water velocity (with an expected mobile water content of $\theta = 0.34$) of 0.0028 cm s^{-1} were used to calculate a mean dispersion coefficient of $0.016 \text{ cm}^2 \text{ s}^{-1}$.

The radiographical projections are shown in Fig. 10 as time series of 1, 5, 15, 20 and 30 min of infiltration ii) (upper row, CaCl₂-solution) and iii) (lower row, KI-solution). Displayed are relative attenuation changes (normalized to highest value) to quantify the region of main solution transport. Density changes overall were higher for the denser KI tracer solution than for the CaCl₂ solution due to stronger X-ray attenuation by the heavy iodine ions (higher atomic number). The relative density changes were attributed to relative changes in liquid content.

Regarding the FC technique itself it is important to note that all flow-analyzing methods indicate that no preferential lateral flow along the FC walls (either front or side walls) was observed for the infiltration experiments. For both infiltration cycles in initially dry material ($\theta = 0.012$) more or less similar flow pathways were observed. Flow occurred preferentially through the sand matrix (density changes 60-100 %) and in the cracks formed during drying in the brownish structure, largely bypassing the brownish structure. Overall higher relative density changes (> 80 %) were observed above the brownish structure. With increasing transport time density changes above the brownish structure increased at the transition zone to the sand matrix. Infiltration fronts in the sand matrix were somehow fringed and not sharp with lower density changes behind the front. This could have been an effect of horizontal distribution of solution during vertical migration of the infiltration front. Overall, the most pronounced density changes were observed in the sand matrix with a maximum (> 80 %) right above the brownish structure. This is another indication that the brownish structure acted as a hydraulic barrier.

After Infiltration, changes in volumetric water content were higher for infiltration iii) with $\theta = 0.29$ than for infiltration ii) with $\theta = 0.24$ after infiltration (different radiographic solution densities were considered). Also the determined area (from image analysis) of density chang-

es > 80 %, were greater for infiltration iii) with 18.2 % than for infiltration ii) with 10.3 %. The flow rate of infiltration ii) was smaller with 1.83 ml min⁻¹ than for infiltration iii) with 2.2 ml min⁻¹ at the beginning of infiltration. At the end of the experiment the respective flow rates decreased to 0.62 ml min⁻¹ for infiltration ii) and to 0.77 ml min⁻¹ for infiltration iii).

In summary, the repeated infiltration experiments, initially into moist and then twice into dry soil, showed geometrically quite similar and reproducible transport patterns, despite possible structural changes, i.e., formation of cracks in the brownish structure due to drying or due to local flow rate differences. The main transport zone was the sand matrix while the brownish structure was mainly excluded from convective liquid transport and thus transport behavior was strongly influenced by soil sample heterogeneities which is indicated already by the visible color of the material. Possible changes in particle surface wetting properties after longer contact with water after the first infiltration had no or only minor influence on the transport processes. The moisture heterogeneity patterns for this sample indicate clearly that structural and textural features rather than wettability (on a very low average water repellency level) govern transport pattern and moisture pattern in the flow cell.

Statistical relationship between parameter

Geostatistical results are summarized in Tab. 3. Results from CA measurements for soil slice D were taken from Krueger and Bachmann (2017). Spherical and exponential models were fitted to semivariograms with r^2 between 0.97 and 0.999. For Sum C-H and in consequence for PWI as well, pure nugget effect was found, i.e. no spatial autocorrelation ranges could be calculated. Thus we excluded this data for further analysis of interrelations between the parameter.

Geostatistical evaluation revealed lowest spatial correlation ranges for enzyme activities of N-Acet with 3.7 cm and highest for Sum Si-O with 7.8 cm. Spatial correlation ranges for

other parameters varied between 4.0 and 5.1 cm. The distances of spatial dependencies were more than ten times higher than the smallest grid measurement distances for all parameters, except of Sum C-H and PWI with pure nugget model. Therefore, the predicted contour plots were suitable to calculate interrelationships between the parameter unless the grid sizes were different and the measurement points were not exactly matching (few mm offset). Soil slices were spatially separated from each other from B to C and C to D of 5 mm and from B to D of 10 mm (Fig. 2). Analysis of enzyme activities and DRIFT measurements had the longest separation distance of 10 mm. Summarized it might be stated that the calculated spatial correlation ranges were greater than the longest separation distance of the soil slices.

The grid measurements had the following offsets in mm compared to a starting point at bottom left of the sample slice ($x=0, y=0$, Fig. 2): Zymography, $x = 4.5 / y = 22$, DRIFT $x = 3 / y = 25$ and CA mapping $x = 5 / y = 25$. All analyzes were made on the right sample surface.

We have reduced all grid sizes to the smallest grid size of CA measurements with $x = 5$ to $x = 61$ and $y = 25$ to $y = 115$ mm and with respect to the offset of each measurement grid. This resulted in 75×112 data points ($n = 8400$) for each parameter. Correlation coefficients are given in Tab. 5 as correlation matrix. The relative strongest correlation were determined between N-Acet and Phos with R^2 0.664 followed by Sum Si-O and Sum C=O with R^2 of 0.539. Also interrelationships were calculated for β -Glu and Phos with R^2 0.429 and CA and Phos with R^2 0.367. Other correlation coefficients were very weak and ranges from 0.00004 to 0.159.

Discussion

Methodological approach

The FC concept can be considered as a first methodological approach to analyze complex processes on the small scale within an intact soil matrix. This procedure can be done with - in principle - undisturbed sample replicates which are quite similar (mm to cm slices) regarding texture and structure. From a visual assessment the soil slices were nearly undisturbed, except when desiccation leads to shrinkage and crack formation. It is worth to note that during the infiltration experiments no lateral or preferential flow occurred along FC walls as a source of possible artifacts during water or solute flux analysis. Visualization of various parameters is considered as one major advantage because this sampling approach allows on one hand easy access to a large sample surface for various 2D analysis techniques of mm-scaled particle surface properties. On the other hand this geometry still works well for defined infiltration experiments which are conducted during our experiment by hanging water column devices to adjust defined unsaturated moisture conditions. Rapid moisture changes can be detected by 2D radiography or by X-ray tomography. This gave the opportunity to analyze micro-hydraulic flow domains to prove assumptions needed to define models for the accessibility of water and nutrients. Further, hydraulic models can well be calibrated to adjust physical assumptions like dual-porosity or dual permeability models (Gerke & van Genuchten, 1993) in conjunction with chemical or biological parameters in spatial resolution of mm. This allows a more realistic access to the living conditions of soil organisms. Also replicates of undisturbed samples are apparently spatial more similar (5 and 10 mm distance) than soil cores taken conventionally at dm distance.

SOM composition and microbial activity

Activities of microorganisms in subsoil are assumed to be limited by easily available and decomposable substrates (quality of OM) and thus C decomposition in subsoil is assumed to be decreased (e.g. Heitkötter et al. 2017) or only patchy distributed (Nunan et al., 2003). In preferential flow pathways SOC and nitrogen concentrations and microbial activity were found to be higher than in the surrounding soil matrix due to a better nutrient supply (Bundt et al., 2001a, b). According to descriptive statistics like standard deviation, scattering of all parameters were more or less in a small range for our subsoil material. However, looking on spatial variability it is evident that values of e.g., Phos, β -Glu, Sum Si-O, and Sum C=O, that were higher than the average are clustered in the region of the brownish structure and within these structural domains are correlated with each other. Also two 'hot spots' of higher enzyme activities were found. This was observed by comparing contour plots and photographs visually. Nunan et al. (2003) found spatial autocorrelation in soil bacterial communities (top- and subsoil) and suggested that bacterial patches may be associated with local deposits of substrate. Nonetheless, not all the statistical relationships have confirmed this assumption when data are strictly attributed to a rigid coordinate system, hence not taking into account a probable shift of soil structural elements along cell A to E. Looking on the potential to unravel coupled bio-chemical-physical spatial processes, our study indicate relationships between measured DRIFT signal intensities of Sum Si-O and Sum C=O (hydrophilic OM functional groups), and domains of enzyme activities of Phos and β -Glu and Phos and N-Acet and also for CA and Phos for the mm-scaled mapping. Bulk parameter C_{bulk} and CA_{bulk} were positively correlated. Measured parameter on the same soil slice were correlated, i.e. between Sum Si-O and Sum C=O and between Phos and β -Glu / N-Acet. The area size of the previously mentioned brownish region increased from left to right (by visible inspection, Fig. 2). This heterogeneously distributed structure maybe responsible for the missing statistical relation-

ship between the measured parameter, i.e. DRIFT and enzyme activities. Texture analyses of 3-cm depth steps for 1-cm increments by Krueger and Bachmann (2017) for the same sampling region revealed increased silt content of 89.4% (clay, 1.1 %, sand 9.5 %) for the brownish region with a decreased silt content of 24 % for the matrix. Also Sum Si-O results of DRIFT measurements, which were indicative for spatial variations in particle size, confirm the assumption of a loamy band in the middle of the soil slices. This was also supported by calculated correlations of Sum Si-O between Band versus MI and MII (DRIFT transects). The statistical evaluation revealed significant differences between Band versus MI and MII, moreover significant differences were higher for MII than for MI. This supports the assumption (by visible inspection) of a region with smaller particles in the brownish colored part, also shown by higher Sum Si-O values in this region. Textural changes within the sample could be assumed as one reason for missing relations between the parameters. The visible differences concerning the brownish structure and the less colored matrix probably led to a heterogeneous OM distribution. Differences in texture and a probably higher Al-/Fe-(hydr)oxide content (the latter visible in the brownish red colored region) resulted in more sorption sites on particle surfaces and to a higher OM abundance of OM functional groups than in the sand matrix leading finally to a more or less intensive concentration of selected exo-enzymes (Phos and β -Glu and Phos and N-Acet). It is also remarkable, that a low structured almost sandy soil domain shows an extended differentiation of measured soil properties, i.e. spatial distribution of OM functional groups and enzyme activities on the observed spatial cm to mm scale.

Repellency effects

For soil slice C, spatial distribution of C_{bulk} , Sum C-H, and Sum C=O groups as well as of the CA_{bulk} values was not always consistent, except for relation between C_{bulk} and CA_{bulk} . The

lack of these plausible correlations can be due to the fact that the C_{bulk} content of the samples was at a very low level. This level could have been responsible for the very small signal intensities of C-H bonds in the DRIFT spectra which often were near the limit of detection (0.02 KM units; Leue et al., 2013). In addition, the CA_{bulk} values were far below the level of water repellency ($< 90^\circ$) what makes a significant relationship to the PWI values difficult (Leue et al., 2015). The found PWI values were lower compared to values found by Leue et al. (2010b) for intact surfaces from Bt-horizons of Luvisols. However, note that the cited work was addressed to OM accumulations in coatings along cracks and biopores acting as preferential flow paths while our work is focused on OM in almost unstructured Cambisol subsoil. However, the overall small PWI values predict potentially high wettability which was confirmed by SDM measurements.

The relationship between surface chemical composition as derived from XPS and bulk CAs of disturbed soil samples is generally known, i.e. surface O/C ratio is negatively and C_{np} content is positively correlated with CAs (Woche et al., 2017). However, in case of our study no correlations were found due to the only small variations in bulk CAs. More patchily distributed hydrophobic compounds (C_{np}) were diluted in the bulk samples, resulting in only small variations in CAs compared to CAs mapped on intact surfaces. CAs mapped on undisturbed surfaces were not directly investigated with XPS because of technical reasons (and differently to DRIFT measurements). This ambiguous result of mapped CA on undisturbed surface and disturbed bulk samples might be supported by other results from sandy forest soil samples with low C content. Water repellency showed a minimum at low total C content while CAs increased from this minimum with lower and with higher C content (Ellerbrock et al., 2005; Bachmann et al., 2016). This effect was explained by a specific layering of amphiphilic organic molecules in thin organic particle coatings. That probably explains the heterogeneously distributed CAs of the mapped soil slice. The higher CAs above the brownish

structure may be a result of hydrophobic OM groups (C backbone chains) which were directed to the interface towards the pore space. High and also low CAs at low DRIFT signal intensities could be an effect of specific layering of amphiphilic organic molecules in thin organic particle coatings creating different wetting properties according to the thickness of the interface. In disturbed bulk soil samples this effect cant not be detected.

Implications for bio-hydrological processes

Dynamic variations in water availability in time and space affect micro-scaled solute transport processes that finally determine the spatial and temporal distribution of microbial communities and activities in soil (Koch, 1990). Dye tracer experiment showed tracer flow mainly in the sand matrix bypassing initially domains with finer texture. After the tracer pulse, rinsing with CaCl_2 -solution led to lower color intensity, while a colored fringe remained in the transition zone sand to the brownish structure (sand to the brownish structure, see photograph 200 and 300 min, Fig. 8) indicating here a less intensive remobilizing potential of the flowing soil solution. Repeated infiltration indicated further a more or less reproduced flow pattern in the same flow path ways used already for BB transport, bypassing again the domains formerly enriched via diffusive BB transport. This indicate in a rather uniformly looking subsoil matrix the occurrence of micro-preferential flow pathways in the cm scale which might have relevance for the local average supply with water and dissolved nutrients. Relative higher dispersion coefficients are attributed to immobile water during unsaturated flow and depend on water content, flow rate, concentration of transported solution and soil type. A simultaneously applied non-reactive tracer (bromide solution) with a reactive dye tracer (BB) may display the non-equilibrium flow characteristics better (Kung et al., 2000).

Studies using radiography were mostly conducted with Hele-Shaw cells or flow chambers with disturbed soil material (e.g. Bayer et al., 2004; Rezanezhad et al., 2006) or were characterized by image analyses (e.g. Wallach et al., 2013) when using thin rectangular experimental setups to conduct a 2D flow field. For our study with undisturbed soil it was more challenging to quantify changes in volumetric water contents by calibrations as e.g. Bayer et al (2004) did in their study. Recently, Weller et al. (2017) presented a methodological approach to quantify water in terms of volumetric water contents in cylindrical undisturbed soil cores via radiography with a sample-specific calibration procedure. This approach may be effectively applicable also with a very low time demand for x-ray scans to our rectangular FC in order to sample information on the flow characteristic of heterogeneous flow fields to select and to calibrate adequate hydraulic models (i. e. Šimůnek et al., 2008).

In general, the textural variations within the sample may have resulted in the formation of favorable or less favorable conditions for microorganisms with respect to water availability with favorable nutrient conditions due to more stagnant water flow in and as well around the finer textured structure. Water-filled pores with dissolved nutrients become less available for microbial utilization below a specific water content, when the soil becomes dry (Frey, 2007).

The physically separation of microorganisms and OM is apparently one of the most important factors leading to the protection and stabilization of SOM in subsoils (Or et al., 2007). It is important to note that this effect seems also to occur due to high variable flow velocities in less structured sandy substrates. It has been shown that low or stagnant flow velocity (flow interruption) enhances significantly the probability for colloid adsorption (Carstens et al., 2017). This process may also support adsorption and thus enrichment of DOC as potential nutrient source for microorganisms on interfaces between regions with abrupt textural changes, which are not necessarily classical aggregate surfaces. Such a process is also indicated in our study due to the high CA domain on and above the textural interface. It is obvious that

this structure acted as a hydraulic barrier for convective flow, but not for diffusion as indicated by BB, suggesting a hydraulic two-flux region model (Gerke & van Genuchten, 1999) for further quantification.

This may cause a longer residence time of DOC above and in this brownish domains. In line, the relative higher OM content (as functional groups detected by DRIFT spectroscopy) in and around the brownish region could favor an increased microbial activity compared to the sand matrix due to the higher density of easy degradable OM. Nonetheless, enzyme activities were not statistically related to the presence of OM functional groups (DRIFT). Additional measurements, e.g. visualization of the distribution of living microorganisms or the origin of OM, may clarify that point which is at present beyond the scope.

The mapped CAs reflected the spatial distribution of potential SWR in the air-dry state within the soil slice surface D and may not directly represent actual wetting properties (influenced by actual moisture content) in our study. Conformational changes of hydrophobic functional groups (Woche et al., 2017) at the solid liquid interface after contact with water, the generally low level of CA observed and reproducible flow field pattern suggest that wettability effects after long periods of water-wetted surfaces and low degree of potential water repellency have minor impact on the infiltration experiments in our study.

Conclusions

Following the results of this study we conclude that the FC concept is a versatile tool to analyze the spatial distribution and finally coupling mechanisms between biological, physico-chemical and chemical particle surface properties including the analysis of non-destructive transport processes on mm to cm scale. This scale might be the most relevant one to understand the coupling of physical and biological processes in real, i.e. undisturbed soil which can

be investigated under controlled lab conditions. In our study we found a general relationship between spatial behavior of CA_{bulk} and C_{bulk} . General tendencies were observed (by visual inspection) between biological, physico-chemical and chemical properties despite the mainly missing statistical interrelationships. The spatial distribution of these parameters and also the 2D transport characteristics in general seem to depend on textural changes in the sample (loamy band in sand matrix).

The FC concept may be improved by additional non-destructive imaging methods which is especially challenging for the detection of small scale textural changes. Comparison of equal soil domains, i.e. sand matrix and loamy band, between the soil slices may improve the relationships between soil properties. Another aspect would be to apply the measurements at opposite soil surfaces of two soil slides such that these two parameters are obtained on soil particles that were directly mirrored.

Further development of non-destructive spectroscopic mapping methods combined with biological and physical imaging methods provides principally a versatile approach, if the observed system is not strongly affected by the sampling techniques itself. In case of the proposed FC technique it has been shown that different methods can be combined via the analysis of undisturbed replicate soil slices to finally unravel living conditions of microorganisms or fine roots in their natural soil environment. In this regard, the FC technique might be a step forward in comparison with conventional sampling techniques having a potential for further development.

Acknowledgements

The authors like to thank the Deutsche Forschungsgemeinschaft DFG for financial support within the Research Group “SUBSOM”, BA1359/604212. We like to thank Martin

Volkman for his technical support during FC construction and Dr. John Maximilian Köhne (Soil Physics Department, UFZ-Halle) for his technical support during radiographical measurements. Also we like to thank Susanne K. Woche for XPS and CA analysis.

Accepted Article

Literature

- Allaire, S.E., S. Roulier, & A.J. Cessna (2009). Quantifying preferential flow in soils: A review of different techniques. *Journal of Hydrology* 378(1-2), 179-204. doi:10.1016/j.jhydrol.2009.08.013
- Bachmann, J., A. Ellies, & K. Hartge (2000). Development and application of a new sessile drop contact angle method to assess soil water repellency. *Journal of Hydrology* 231-232, 66–75. doi: 10.1016/S0022-1694(00)00184-0
- Bachmann, J., M.-O. Goebel, & S.K. Woche (2013). Small-scale contact angle mapping on undisturbed soil surfaces. *Journal of Hydrology and Hydromechanics* 61, 3-8. doi: 10.2478/johh-2013-0002
- Bachmann, J., J. Krueger, M.-O. Goebel, & S. Heinze (2016). Occurrence and spatial pattern of water repellency in a beech forest subsoil. *Journal of Hydrology and Hydromechanics* 64(2), 100–110. doi:10.1515/johh-2016-0005
- Bauters, T., T. Steenhuis, D. DiCarlo, J. Nieber, L.W. Dekker, C. Ritsema, J.-Y. Parlange, & R. Haverkamp (2000). Physics of water repellent soils. *Journal of Hydrology* 231-232, 233–243. doi: 10.1016/S0022-1694(00)00197-9
- Bayer, A., H.-J. Vogel, & K. Roth (2004). Direct measurement of the soil water retention curve using X-ray absorption. *Hydrology and Earth System Sciences Discussions* 8(1), 2–7.
- Bisdorf, E.B.A., L.W. Dekker, & J.F.Th. Schoute (1993). Water repellency of sieve fractions from sandy soils and relationships with organic material and soil structure. *Geoderma* 56(1-4), 105–118. doi: 10.1016/0016-7061(93)90103-R
- Buczko, U., O. Bens, & R.F. Hüttl (2005). Variability of soil water repellency in sandy forest soils with different stand structure under Scots pine (*Pinus sylvestris*) and beech (*Fagus sylvatica*). *Geoderma* 126, 317–336. doi: 10.1016/j.geoderma.2004.10.003

- Bundt, M., M. Jaggi, P. Blaser, R. Siegwolf, & F. Hagedorn (2001a). Carbon and Nitrogen Dynamics in Preferential Flow Paths and Matrix of a Forest Soil. *Soil Science Society of America Journal* 65, 1529–1538. doi:10.2136/sssaj2001.6551529x
- Bundt, M., F. Widmer, M. Pesaro, J. Zeyer, & P. Blaser (2001b). Preferential flow paths: biological ‘hot spots’ in soils. *Soil Biology and Biochemistry* 33, 729–738. doi: 10.1016/S0038-0717(00)00218-2
- Burns, R.G., J.L. DeForest, J. Marxsen, R.L. Sinsabaugh, M.E. Stromberger, M.D. Wallenstein, M.N. Weintraub, & A. Zoppini (2013). Soil enzymes in a changing environment: Current knowledge and future directions. In *Soil Biology and Biochemistry* 58, pp. 216–234. doi: 10.1016/j.soilbio.2012.11.009
- Caldwell, B.A. (2005). Enzyme activities as a component of soil biodiversity: A review. *Pedobiologia* 49(6), pp. 637–644. doi: 10.1016/j.pedobi.2005.06.003
- Capriel, P., T. Beck, H. Borchert, J. Gronholz, & G. Zachmann (1995). Hydrophobicity of the organic matter in arable soils. *Soil Biology and Biochemistry* 17, 1453–1458. doi: 10.1016/0038-0717(95)00068-P
- Carstens, J.F., J. Bachmann, & I. Neuweiler (2017). Effects of flow interruption on transport and retention of iron oxide colloids in quartz sand. *Colloids and Surfaces A: Physico-chemical and Engineering Aspects* 520, 532-543. doi: 10.1016/j.colsurfa.2017.02.003
- Chan, K.Y. (1990). Development of Seasonal Water Repellence under Direct Drilling. *Soil Science Society of America Journal* 56(1), 326-329. doi: 10.2136/sssaj1992.-03615995005600010054x
- Chenu, C., Y. Le Bissonnais, & D. Arrouays (2000). Organic Matter Influence on Clay Wettability and Soil Aggregate Stability. *Soil Science Society of America Journal* 64, 1479–1486. doi: 10.2136/sssaj2000.6441479x

- Clothier, B., I. Vogeler, & G.N. Magesan (2000). The breakdown of water repellency and solute transport through a hydrophobic soil. *Journal of Hydrology* 231-232, 255-264. doi: 10.1016/S0022-1694(00)00199-2
- Dekker, L.W., S.H. Doerr, K. Oostindie, A.K. Ziogas, & C.J. Ritsema (2001). Water Repellency and Critical Soil Water Content in a Dune Sand. *Soil Science Society of America Journal* 65, 1667–1674. doi:10.2136/sssaj2001.1667
- Dekker, L.W., & C.J. Ritsema (1994). How water moves in a water repellent sandy soil 1. Potential and actual water repellency. *Water Resources Research* 30, 2507–2517. doi: 10.1029/94WR00749
- Doerr, S.H., R.A. Shakesby, & R. Walsh (2000). Soil water repellency: its causes, characteristics and hydro-geomorphological significance. *Earth-Science Reviews* 51(1-4), 33–65. doi: 10.1016/S0012-8252(00)00011-8
- Doerr, S.H., A.J.D. Ferreira, R.P.D. Walsh, R.A. Shakesby, G. Leighton-Boyce, & C.O.A. Coelho (2003). Soil water repellency as a potential parameter in rainfall-runoff modeling: experimental evidence at point to catchment scales from Portugal. *Hydrological Processes* 17(2), 363-377. doi: 10.1002/hyp.1129
- Ellerbrock, R.H., H.H. Gerke, J., Bachmann, & M.-O. Goebel (2005). Composition of Organic Fractions for Explaining Wettability of Three Forest Soils. *Soil Science Society of America Journal* 69, 57–66. doi:10.2136/sssaj2005.0057
- Frey, S.D. (2007). Spatial distribution of soil microorganisms. In Paul, E.A. (Eds.), *Soil Microbiology, Ecology, and Biochemistry*, 3rd Edition. Academic Press, Elsevier, USA, pp. 283-300.
- Germán, J., & M. Flühler (2000). Sorption of Brilliant Blue FCF in soils as affected by pH and ionic strength. *Geoderma* 97, 87-101. doi: 10.1016/S0016-7061(00)00027-6.

- Gercke, H.H., & M.T. van Genuchten (1993). A dual-porosity model for simulating the preferential movement of water and solutes in structured porous media. *Water Resources Research* 29(2), 305-319. doi: 10.1029/92WR02339
- Goebel, M.-O., J. Bachmann, M. Reichstein, I.A. Janssens, & G. Guggenberger (2011). Soil water repellency and its implications for organic matter decomposition – is there a link to extreme climatic events? *Global Change Biology* 17, 2640-2656. doi: 10.1111/j.1365-2486.2011.02414.x
- Goebel, M.-O., S.K. Woche, P.M. Abraham, G.E. Schaumann, & J. Bachmann (2013). Water repellency enhances the deposition of negatively charged hydrophilic colloids in a water-saturated sand matrix. *Colloids and Surfaces A: Physicochemical and Engineering Aspects* 431, 150-160.
- Goebel, M.-O., S.K. Woche, J. Bachmann, A. Lamparter, & W.R. Fischer (2007). Significance of Wettability-Induced Changes in Microscopic Water Distribution for Soil Organic Matter Decomposition. *Soil Science Society of America Journal* 71(5), 1593. doi: 10.1016/j.colsurfa.2013.04.038
- Hallett, P.D., J. Bachmann, H. Czachor, E. Urbanek, & Z. Bin Zhang (2010). Hydrophobicity of soil. In: Glinski J., Horabik, J., & Lipiec J. (Eds.), *Encyclopedia of Agrophysics*, Springer, pp. 378–383.
- Heitkötter, J., J. Niebuhr, S. Heinze, & B. Marschner (2017). Patterns of nitrogen and citric acid induced changes in C-turnover and enzyme activities are different in topsoil and subsoil of a sandy Cambisol. *Geoderma* 292, 111-117.
- Horne, D.J., & J.C. McIntosh (2000). Hydrophobic compounds in sands in New Zealand – extraction, characterization and proposed mechanisms for repellency expression. *Journal of Hydrology* 231-232, 35-46. doi: 10.1016/S0022-1694(00)00181-5

IUSS Working Group WRB (2014). World Reference Base for Soil Resources 2014. International soil classification system for naming soils and creating legends for soil maps. *World Soil Resources Reports No. 106*. FAO, Rome.

Koch, A.L. (1990). Diffusion the crucial process in many aspects of the biology of bacteria. In: Marshall KC (ed). *Advances in Microbial Ecology*. Boston, MA: Springer, 1990, 37–70.

Kung, K.-J.S., E.J. Klavivko, T.J. Gish, T.S. Steenhuis, G. Bubenzer, & C.S. Helling (2000). Quantifying Preferential Flow by Breakthrough of Sequentially Applied Tracers Silt Loam Soil. *Soil Science Society of America Journal* 64, 1296-1304. doi:10.2136/sssaj2000.6441296x

Krueger, J., J. Böttcher, C. Schmunk, & J. Bachmann (2016). Soil water repellency and chemical soil properties in a beech forest soil - Spatial variability and interrelations. *Geoderma* 271, 50-62. doi: 10.1016/j.geoderma.2016.02.013

Krueger, J., & J. Bachmann (2017). New field sampling method to analyze spatial distribution of small-scale soil particle surface properties and processes in intact soil. *Vadose Zone Journal* 16(11). doi:10.2136/vzj2017.06.0116

Lamparter, A., J. Bachmann, & S.K. Woche (2010). Determination of Small-Scale Spatial Heterogeneity of Water Repellency in Sandy Soils. *Soil Science Society of America Journal* 74, 2010–2012. doi:10.2136/sssaj2010.0082N

Leue, M., R.H. Ellerbrock, D. Bänninger, & H.H. Gerke (2010a). Impact of Soil Microstructure Geometry on DRIFT Spectra: Comparisons with Beam Trace Modeling. *Soil Science Society of America Journal* 74, 1976-1986. doi:10.2136/sssaj2009.0443

Leue, M., R.H. Ellerbrock, & H.H. Gerke (2010b). DRIFT Mapping of Organic Matter Composition at intact Soil Aggregate Surface. *Vadose Zone Journal* 9(2), 317-324. doi:10.2136/vzj2009.0101

- Leue, M., H.H. Gerke, & R.H. Ellerbrock (2013). Millimetre-scale distribution of organic matter composition at intact biopore and crack surfaces. *European Journal of Soil Science* 64, 757–769. doi:10.1111/ejss.12098.
- Leue, M., H.H. Gerke, & S.C. Godow (2015). Droplet infiltration and organic matter composition of intact crack and biopore surfaces from clay-illuvial horizons. *Journal of Plant Nutrition and Soil Science* 178, 250-260. doi:10.1002/jpln.201400209
- Mao, J., K.G.J. Nierop, J.S. Sinninghe Damsté, & S.C. Dekker (2014). Roots induce stronger soil water repellency than leaf waxes. *Geoderma* 232-234, 328–340. doi:10.1016/j.geoderma.2014.05.024
- Ma'shum, M., & V.C. Farmer (1985). Origin and assessment of water repellence of a sandy south Australian soil. *Australian Journal of Soil Research* 23, 623-626.
- McGhie, D.A., & A.M. Posner (1980). Water Repellence of a Heavy-textured Western Australian Surface Soil. *Australian Journal of Soil Research* 18(3), 309-323. doi:0.1071/SR9800309
- Nielsen, D.R. & O. Wendroth (2003). Spatial and temporal statistics. *Geo Ecology textbook, Catena Verlag, Germany*, pp. 398.
- Nunan, N., K. Wu, I.M. Young, J. W. Crawford, & K. Ritz (2003). Spatial distribution of bacterial communities and their relationships with the micro-architecture of soil. *FEMS Microbiology Ecology* 44, 203-215. doi:10.1016/S0168-6496(03)00027-8
- Okada, K., Y. Kameshima, & A. Yasumori (1998). Chemical Shifts of Silicon X-ray Photoelectron Spectra by Polymerization Structures of Silicates. *Journal of American Ceramic Society* 81, 1970–1972.
- Or, D., B.F. Smets, J.M. Wraith, A. Dechesné, & S.P. Friedman (2007). Physical constraints affecting bacterial habitats and activity in unsaturated porous media – a review. *Advances in Water Resources* 30(6-7), 1505–1527. doi: 10.1016/j.advwatres.2006.05.025

- Rezanezhad, F., H.-J. Vogel, & K. Roth (2006). Experimental study of fingered flow through initially dry sand. *Hydrology and Earth System Sciences Discussions* 3, 2595–2620.
- Schindelin, J., I. Arganda-Carreras, E. Frise, V. Kaynig, M. Longair, T. Pietzsch, S. Preibisch, C. Rueden, S. Saalfeld, B. Schmid, J.-Y. Tinevez, D.J. White, V. Hartenstein, K. Eliceiri, P. Tomancak, & A. Cardona (2012). Fiji: an open-source platform for biological-image analysis. *Nature methods* 9(7), 676-682. doi: 10.1038/nmeth.2019.
- Šimůnek, J., M. Köhne, R. Kodešová, & M. Šejna (2008). Simulating nonequilibrium movement of water, solutes and particles using HYDRUS – a review of recent applications. *Soil and Water Research* 3, 52-51. doi: 10.17221/1200-SWR
- Šimůnek, J., M.Th. van Genuchten, M. Šejna, N. Toride, & F. J. Leij (1999). The STANMOD computer software for evaluating solute transport in porous media using analytical solutions of convection-dispersion equation. Versions 1.0 and 2.0, IGWMC - TPS - 71, International Ground Water Modeling Center, Colorado School of Mines, Golden, Colorado, 32 pp.
- Spohn, M., & Y. Kuzyakov (2014). Spatial and temporal dynamics of hotspots of enzyme activity in soil as affected by living and dead roots-a soil zymography analysis. *Plant and Soil* 379(1-2), 67–77. doi: 10.1016/j.soilbio.2012.12.004.
- Täumer, K., H. Stoffregen, & G. Wessolek (2005). Determination of repellency distribution using soil organic matter and water content. *Geoderma* 125(1-2), 107–115. doi: 10.1016/j.geoderma.2004.07.004
- Thecon, R., & D. Or (2017). Biophysical processes supporting the diversity of microbial life in soil. *FEMS Microbiology Reviews* 41, 599-623. doi: 10.1093/femsre/fux039
- Thévenaz, P., U.E. Ruttimann, & M. Unser (1998). A Pyramid Approach to Subpixel Registration Based on Intensity. *IEEE Transactions on Image Processing* 7(1), 27-41. doi: 10.1109/83.650848

- Tietjen, T., & R.G. Wetzel (2003). Extracellular enzyme–clay mineral complexes: enzyme adsorption, alteration of enzyme activity, and protection from photodegradation. *Aquatic Ecology* 37, 331–339. doi.org/10.1023/B:AECO.0000007044.52801.6b
- Woche, S.K., M.-O. Goebel, M.B. Kirkham, R. Horton, R.R. van der Ploeg, & J. Bachmann (2005). Contact angle of soils as affected by depth, texture, and land management. *European Journal of Soil Science* 56(2), 239–251. doi:10.1111/j.13652389.2004.-00664.x
- Woche, S.K., M.-O. Goebel, R. Mikutta, C. Schurig, M. Kaestner, G. Guggenberger, & J. Bachmann (2017). Soil wettability can be explained by the chemical composition of particle interfaces - An XPS study. *Scientific Reports* 7, 42877. doi:10.1038/srep42877
- Weller, U., F. Leuther, S. Schlüter, & H.-J. Vogel (2017). Quantitative analysis of water infiltration in soil cores using X-ray. *Vadose Zone Journal*. doi: 10.2136/vzj2016.12.0136
- Wallach, R., M. Margolis, & E.R. Graber (2013). The role of contact angle on unstable flow formation during infiltration and drainage in wettable porous media. *Water Resources Research* 49, 6508–6521. doi:10.1002/wrcr.20522, 2013
- Webster, R., & M.A. Oliver (2001). Geostatistics for environmental scientists. *John Wiley & Sons*, Chichester, England, pp. 271.

Tab. 1: Characterization (SOC, soil organic carbon content) of the Dystric Cambisol at site Grindervald. Data were taken from Bachmann et al. (2016).

Soil horizon		SOC	Sand	Silt	Clay
(cm)		(g kg ⁻¹)*100		(%)	
0-2	AE	27	70	26	4
2-12	Bsw	17	65	30	5
12-36	Bw	7	67	29	4
36-65	BwC	3	73	24	3
65-125	C	0.4	95	4	1
125-150	2C	0.1	81	11	8
150-180	2Cg	0.8	72	19	9
180	3C	< 0.1	95	4	1

Accepted

Tab. 2: Semivariogram parameters were given for: i) zymography of soil slice B with enzyme activities of β -glucosidase (β -Glu), N-acetylglucosaminidase (N-Acet) and phosphatase (Phos). ii) summed signal intensities of diffuse reflectance infrared Fourier transform (DRIFT) spectroscopy of soil slice C of Si-O (wave number (WN) 1983 cm^{-1} and WN 1873 cm^{-1}) and the potential wettability index (PWI) as the ratio between DRIFT signal intensities of summed C-H (Sum C-H, WN 2948-2920 cm^{-1} and 2864-2849 cm^{-1}) and the signals of summed C=O (Sum C=O, WN 1720-1700 cm^{-1} and 1625-1600 cm^{-1}). iii) contact angle (CA) measurements on soil slice D.

Sample / Analysis		Model	Semivariogram			Range (cm)	
			r^2	Nugget	Sill		
B	Zymography	β -Glu	spherical	0.998	0.23	7.51	4.2
		N-Acet	spherical	0.998	0.09	2.58	3.7
		Phos	spherical	0.999	0.01	9.70	4.0
C	DRIFT	Sum Si-O	spherical	0.997	0.00102	0.00871	7.8
		Sum C-H	spherical	0.976	0.0021	0.0046	3.1
		Sum C=O	spherical	0.995	9.60	26.77	5.1
		PWI	pure nugget			-	
D	CA	exponential	0.970	109	692	5.4	

Tab. 3: Diffuse reflectance infrared Fourier transform (DRIFT) spectroscopy were measured on soil slice C in 3 horizontal lines ($n = 13$), above the brownish region (MI), in (Band) and under the brownish region (MII). Mean values of summed bands of wave number (WN) 1983 cm^{-1} and 1873 cm^{-1} (Sum Si-O) and the potential wettability index (PWI) as the ratio between DRIFT signal intensities of summed C-H (Sum C-H, WN $2948\text{-}2920 \text{ cm}^{-1}$ and $2864\text{-}2849 \text{ cm}^{-1}$) and the signals of summed C=O (Sum C=O, WN $1720\text{-}1700 \text{ cm}^{-1}$ and $1625\text{-}1600 \text{ cm}^{-1}$) were given with standard deviation (\pm , cursive). Higher PWI values indicate lower wettability. Statistical differences were tested with t-Test for normally distributed data and Mann-Whitney Rank Sum Test (underlined) for non-normally distributed data was performed and was given in p -values.

	Sum Si-O	Sum C-H	Sum C=O	PWI
horizontal lines, meanvalue				
MI	0.806 ± 0.046	0.002 ± 0.001	1.087 ± 0.079	$0.002 \pm 8E-04$
Band	0.886 ± 0.079	0.002 ± 0.001	1.215 ± 0.100	$0.002 \pm 5E-04$
MII	0.756 ± 0.039	0.001 ± 0.000	1.039 ± 0.057	$0.001 \pm 4E-04$
p -Value				
MI/MII	0.007	<u>0.081</u>	<u>0.089</u>	<u>0.397</u>
MI/Band	<0.001	0.756	0.001	<u>0.661</u>
MII/Band	<0.001	0.024	<0.001	<u>0.066</u>
$n=13$, t-Test, <u>Mann-Whitney Rank Sum Test</u>				

Tab. 4: Surface chemical composition was analyzed by X-ray photoelectron spectroscopy for bulk subsamples of soil slice C. Surface C concentrations, amount of polar C (C_p) and nonpolar C (C_{np}) compounds are given in atomic-% (at.-%) as the mean of 3 measurements ($n = 3; \pm$ SD, standard deviation). Ratio of surface O and C concentrations are given as O/C. Contact angles (CA_{bulk}) were determined on disturbed bulk material of subsamples of soil slice C (12 readings).

Sub-sample	C	C_p (at.-%) / SD	C_{np}	C_{np} of C (%)	O/C (-) / SD	CA_{bulk} (°) / SD
1	17.4 \pm 0.23	10.2 \pm 0.63	7.20 \pm 0.76	41.40	3.37 \pm 0.06	64.7 \pm 7.58
3	14.7 \pm 0.49	9.64 \pm 0.61	5.07 \pm 0.62	34.47	4.13 \pm 0.15	32.7 \pm 2.82
4	15.6 \pm 0.49	10.3 \pm 0.43	5.22 \pm 0.38	33.56	2.88 \pm 0.13	53.8 \pm 9.92
8	20.0 \pm 0.13	17.7 \pm 0.84	2.26 \pm 0.71	11.30	2.85 \pm 0.02	51.2 \pm 8.55
12	20.9 \pm 0.52	13.7 \pm 0.27	7.18 \pm 0.44	34.31	2.69 \pm 0.09	60.8 \pm 10.1

Tab. 5: Correlation coefficients (Pearson, R^2) were calculated between parameters given in correlation matrix. i) zymography of soil slice B with enzyme activities of β -glucosidase (β -Glu), N-acetylglucosaminidase (N-Acet) and phosphatase (Phos). ii) summed signal intensities of 2D diffuse reflectance infrared Fourier transform (DRIFT) spectroscopy of soil slice C of Si-O (wave number (WN) 1983 cm^{-1} and WN 1873 cm^{-1}) and signals of summed C=O (Sum C=O, WN 1720-1700 cm^{-1} and 1625-1600 cm^{-1}). iii) contact angle (CA) measurements on soil slice D (data from Krueger & Bachmann, 2017).

		DRIFT		Zymography			CA
		Sum Si-O	Sum C=O	β -Glu	N-Acet	Phos	
		R^2					
DRIFT	Sum Si-O	-	0.539	0.002	0.012	0.076	0.019
	Sum C=O	0.539	-	0.021	0.00004	0.159	0.016
Zymography	β -Glu	0.002	0.021	-	0.053	0.429	0.085
	N-Acet	0.012	0.00004	0.085	-	0.083	0.083
	Phos	0.076	0.159	0.429	0.664	-	0.367
CA		0.019	0.016	0.085	0.083	0.367	-

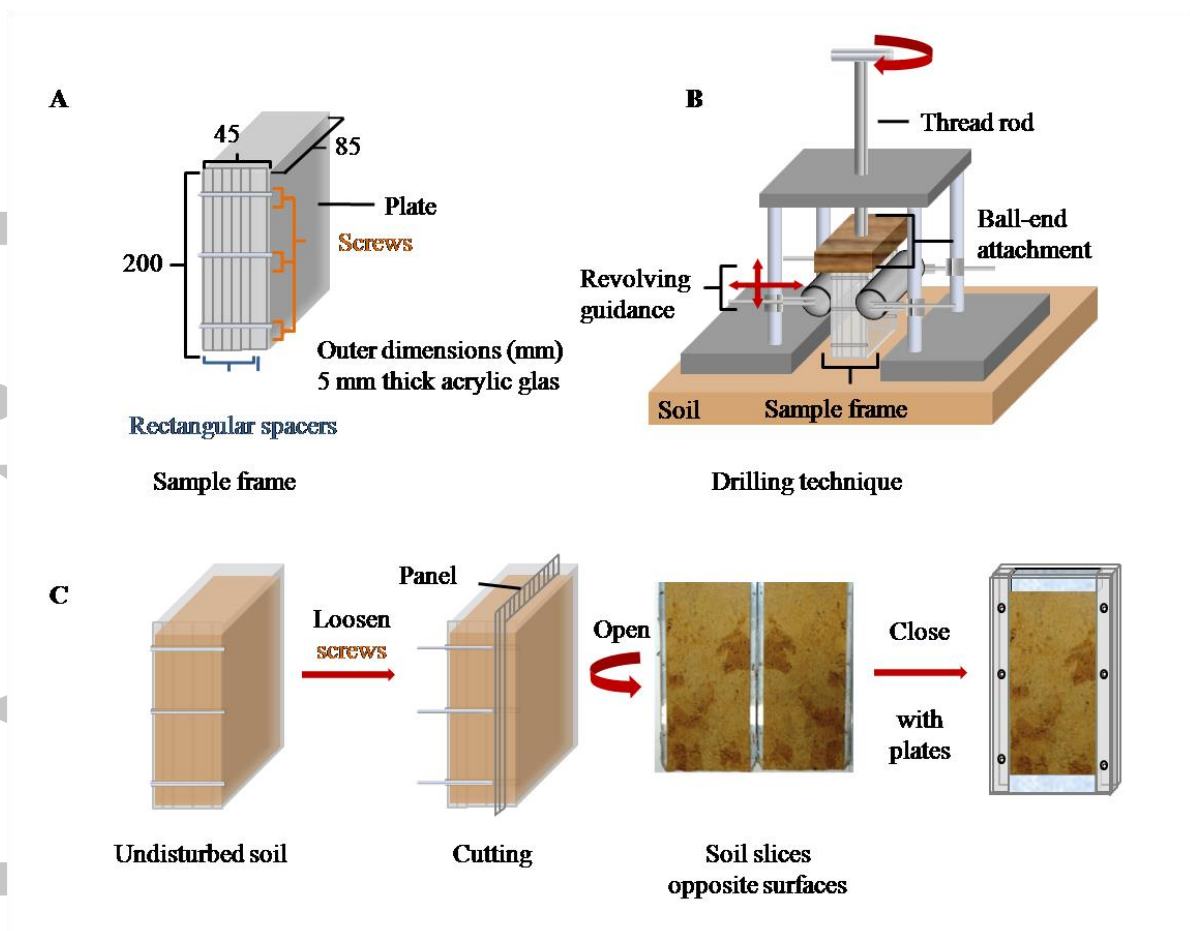


Fig. 1: Flow cell setup: A: Sampling frame. B: Continuously adjustable thread rod connected with a ball-bearing adjusted at the upper attachment of the sampling frame and adjustable revolving guidance at each side of the sampling box. C: Cutting and preparation of soil slices in the laboratory. (Figure was taken from Krueger and Bachmann, 2017, and was slightly modified).

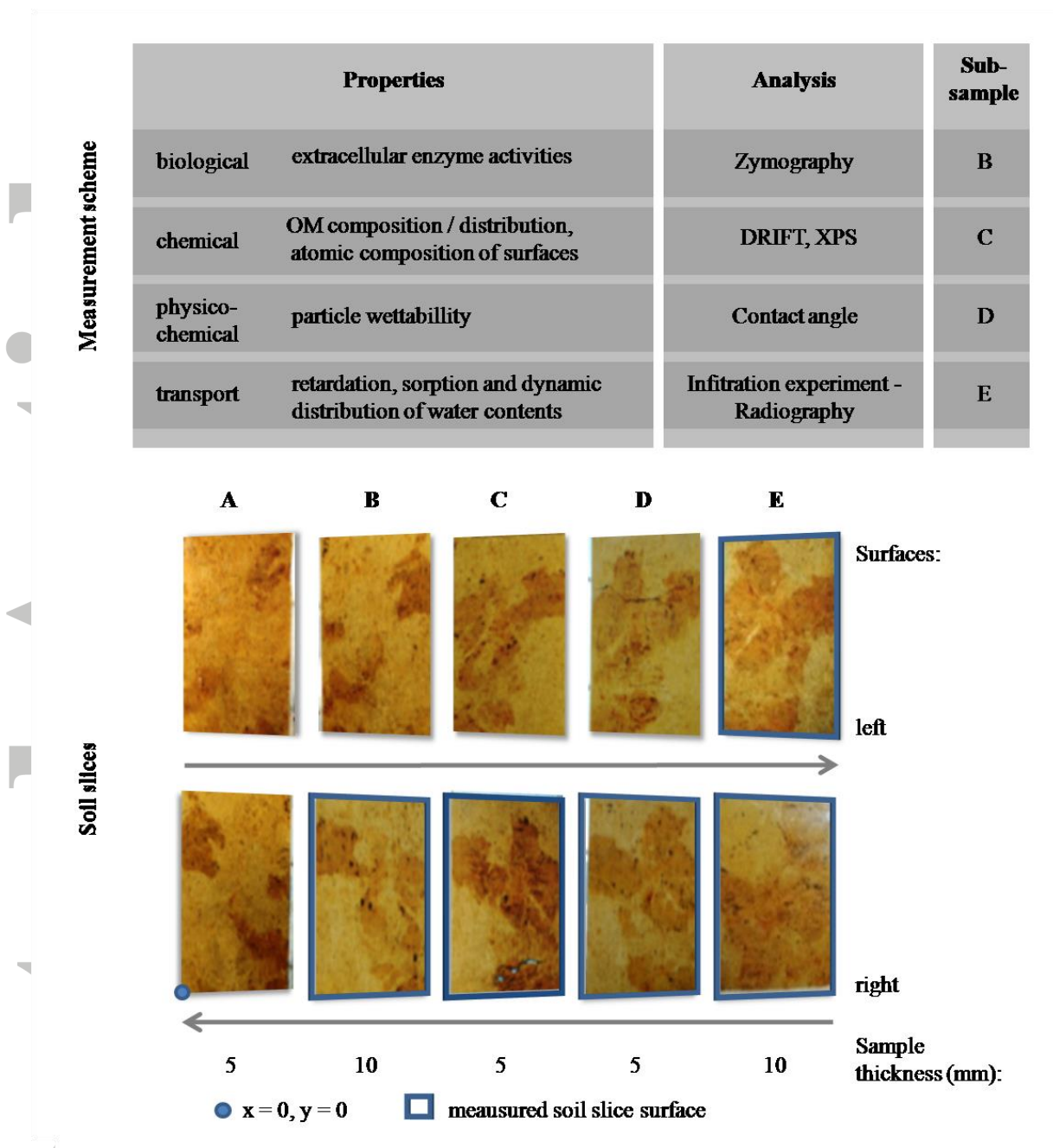


Fig. 2: Measurement scheme and cut surfaces of sample slices, presented as photographs of left and right side of the soil slices. Marked in blue frame: soil slices used for analysis (see measurement scheme). Blue point: reference point of coordinate system.

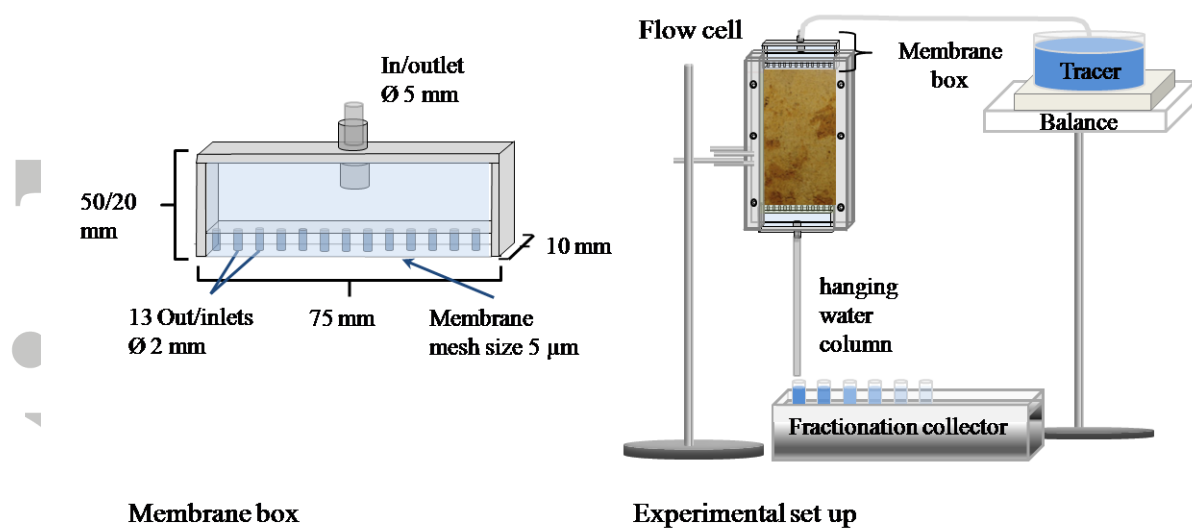


Fig. 3: Experimental set up of dye tracer experiment. Right: Detail of the membrane box which was inserted at the top and bottom of the flow cell.

Accepted

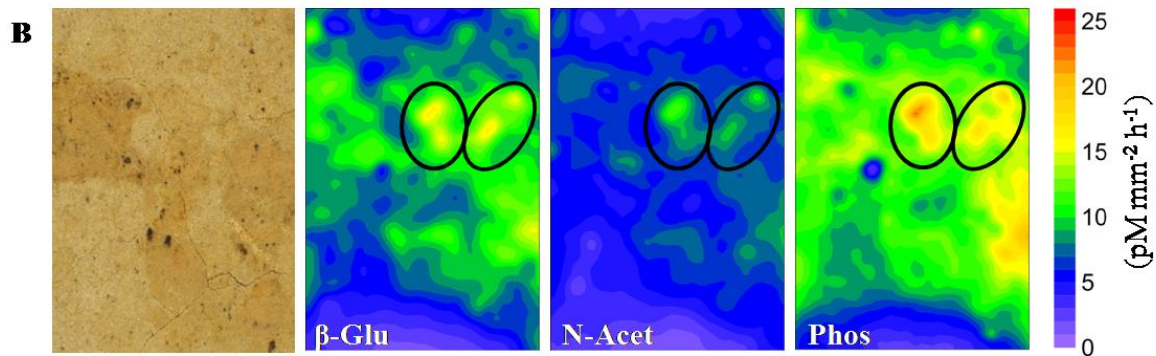


Fig. 4: The spatial distribution of enzyme activities as measured on the surface of soil slice B (see photograph left). Activity of β -glucosidase (β -Glu), N-acetylglucosaminidase (N-Acet) and acid phosphatase (Phos) were analyzed by zymography. Marked in black: regions with increased enzyme activity (slice B, 75 x 100 x 10 mm).

Accepted Article

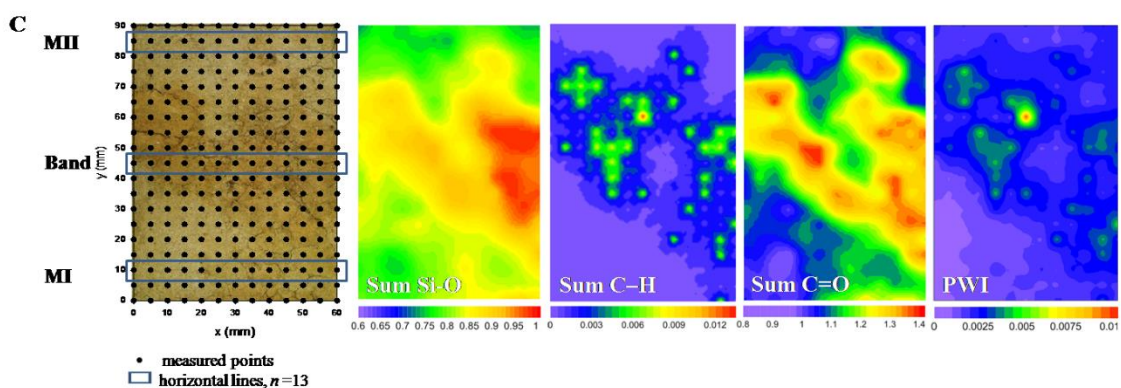


Fig. 5: 2D diffuse reflectance infrared Fourier transform (DRIFT) spectroscopy mapping of soil slice C. Grid size: 60 x 90 mm in 5 mm steps (black points in photograph), resolution 4 cm^{-1} . Summed Si-O (Sum Si-O), summed C-H (Sum C-H) and summed C=O (Sum C=O) is given in Kubelka-Munk (KM) units. The potential wettability index (PWI) is the summed C-H to summed C=O ratio, lower values indicate higher potential wettability.

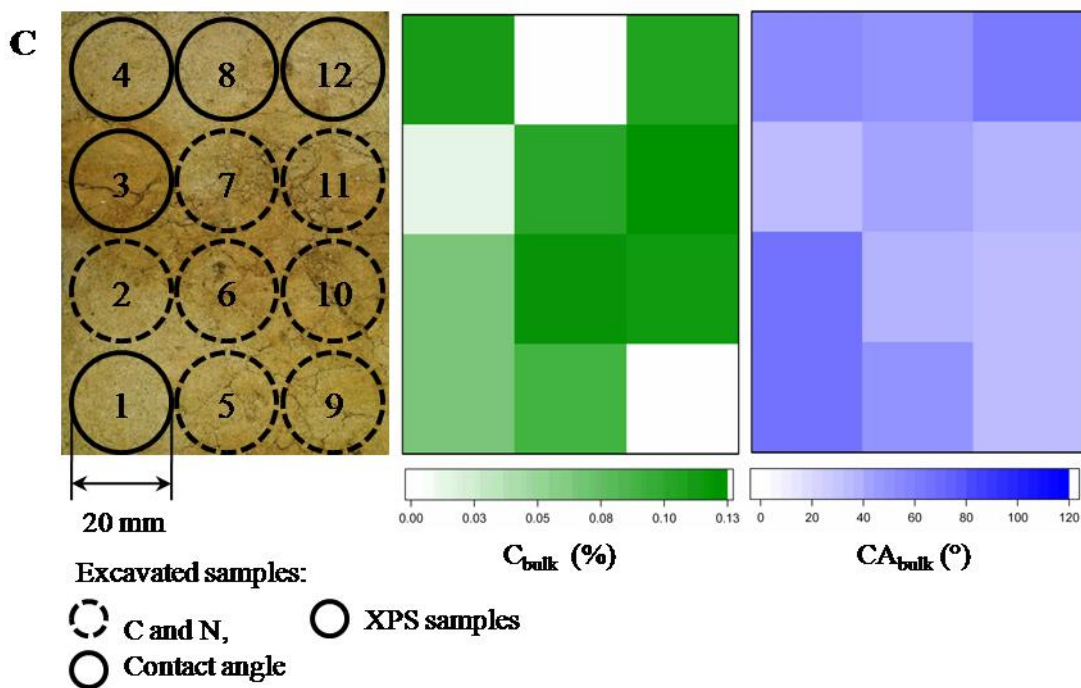


Fig. 6: Left: Photograph of soil slice C. Black and dotted circles show the sampling position of excavated bulk subsamples for analysis of bulk C (C_{bulk}) and N content, contact angles (CA_{bulk}), and surface elemental composition. Surface elemental composition was analyzed by X-ray photoelectron spectroscopy (XPS, black circle) for excavated bulk samples 1, 3, 4, 8, and 12. Right: Results of C_{bulk} and CA_{bulk} determination. N contents were too low and thus are not shown.

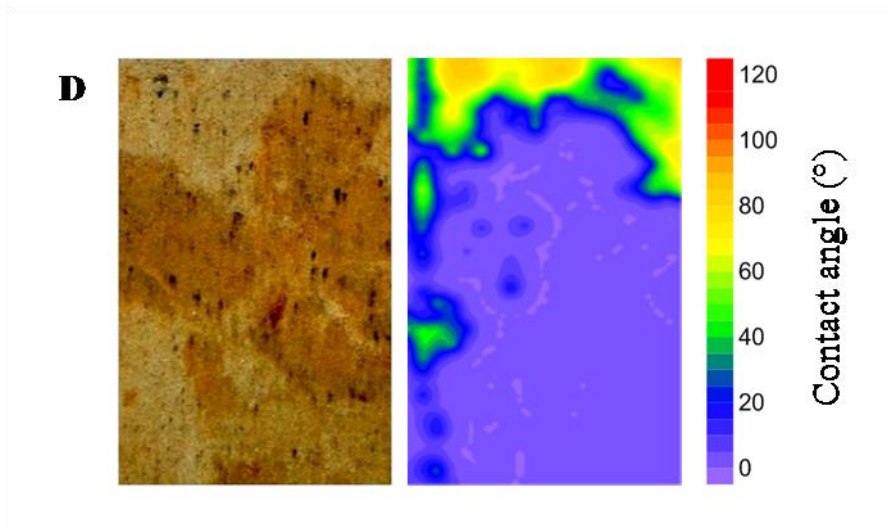


Fig. 7: Contact angle mapping for soil slice D (left, photograph) (Figure taken from Krueger and Bachmann, 2017).

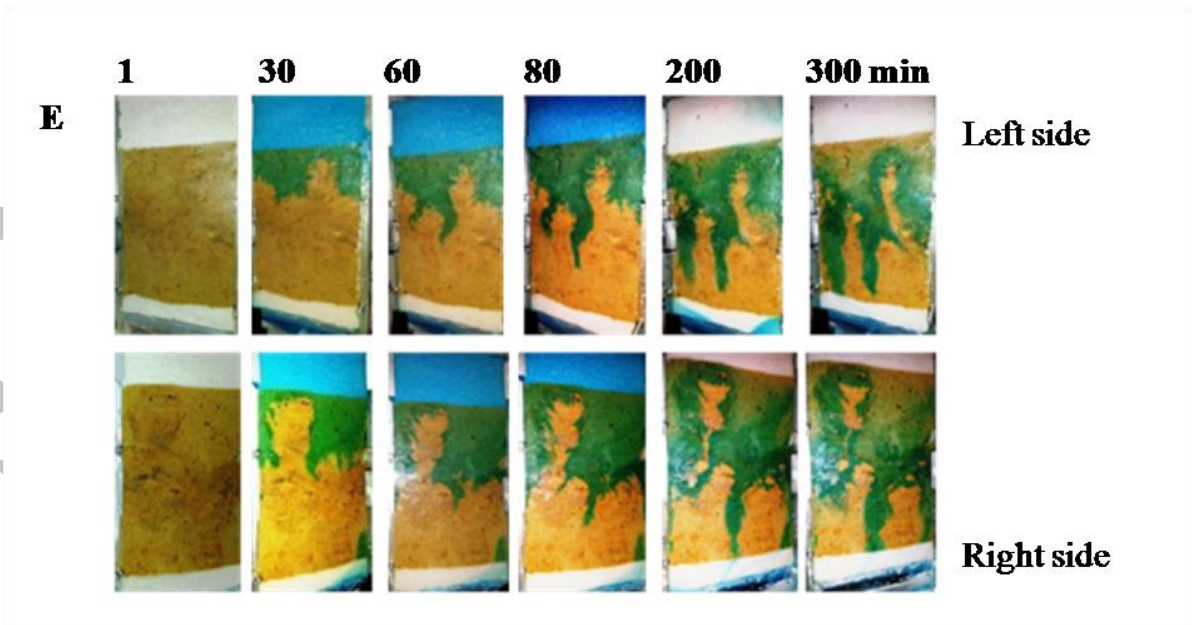


Fig.8: Photographs show dye transport (left and right side of sample surface E) after 1, 30, 60, 80, 200 and 300 min of infiltration.

Accepted

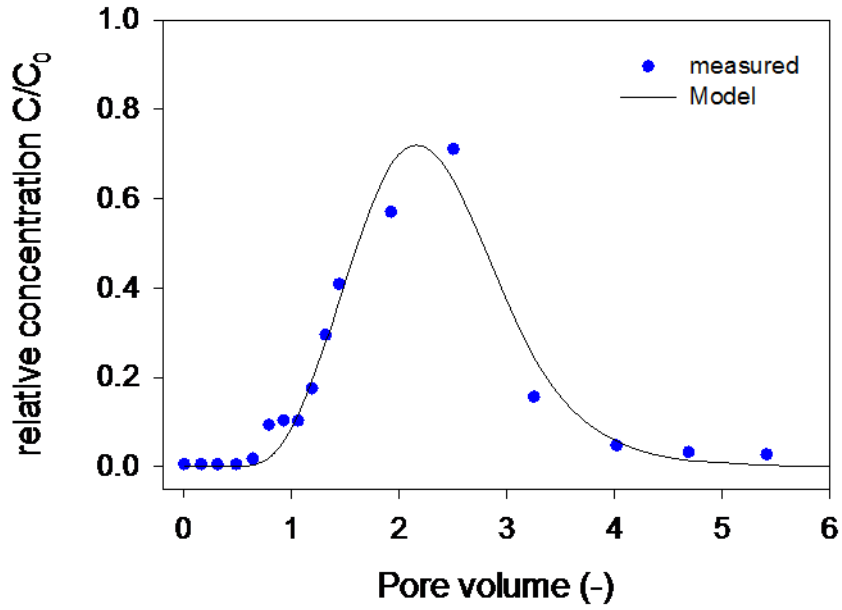


Fig. 9: Breakthrough curve conducted for subsample E with a 1 pore volume-pulse application of dye tracer Brilliant Blue. Relative concentrations (C/C_0) were plotted against eluted pore volume. Blue circles are measured data and the black line are fitted model data (STANMOD, Šimůnek et al., 1999).

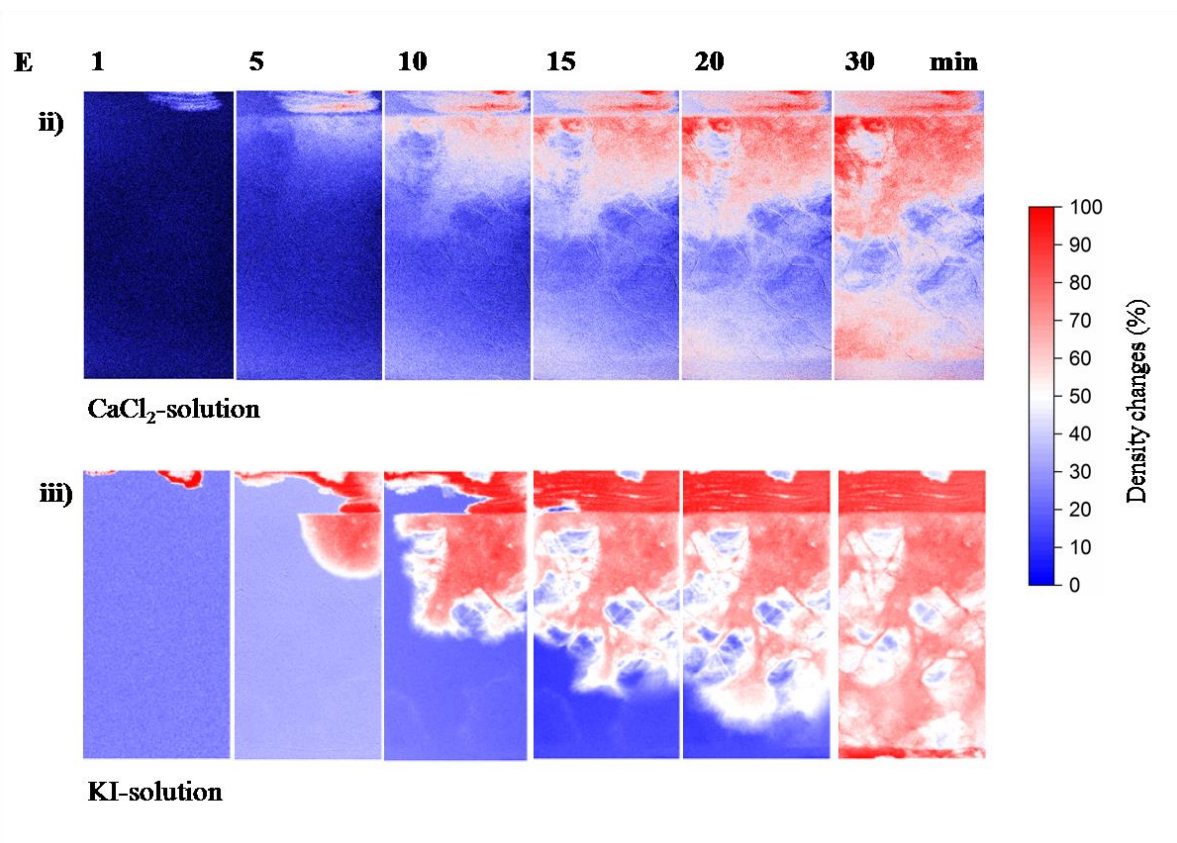


Fig. 10: Radiography: Two infiltration experiments were conducted for soil slice E. I: infiltration of CaCl_2 -solution ii) in initially dry soil. II: After drying, infiltration iii) of KI-solution in initially dry soil. Radiographical images were converted to relative density changes. Images were shown after 1, 5, 10, 15, 20, and 30 min of infiltration.

Accepted